GEOPHYSICS, VOL. 53, NO. 3 (MARCH 1988); P. 304–313, 5 FIGS.

Reflection seismology over azimuthally anisotropic media

Leon Thomsen*

ABSTRACT

Recent surveys have shown that azimuthal anisotropy (due most plausibly to aligned fractures) has an important effect on seismic shear waves. Previous work had discussed these effects on VSP data; the same effects are seen in surface recording of reflections at small to moderate angles of incidence. The anisotropic effects on different polarization components of vertically traveling shear waves permit the recognition and estimation of very small degrees of azimuthal anisotropy (of order ≥ 1 percent), as in an interferometer. Anisotropic effects on traveltime yield estimates of anisotropy which are averages over large depth intervals. Often, raw field data must be corrected for these effects before the reflectors may be imaged; two variations of a rotational algorithm to determine the "principal time series" are derived. Anisotropic effects on moveout lead to abnormal moveout unless the survey line is parallel to the fractures. Anisotropic effects on reflection amplitude permit the recognition and estimation of anisotropy (hence fracture intensity) differences at the reflecting horizon, i.e., with high vertical resolution.

INTRODUCTION

It has become apparent over the last several years that most upper-crustal rocks are azimuthally anisotropic to some degree. Crampin (1984a) and references therein provide a good review of such evidence, evidence taken mainly outside the context of exploration seismology. Crampin (1984b, 1985a) provides a clear account of the importance of azimuthal anisotropy to exploration and its effects on vertical seismic profile (VSP) data. The emphasis on subsurface data was intentional, as "the surface imposes its own anomalies on the polarizations of the incident shear wave. This makes analysis of anisotropy-induced polarization anomalies particularly difficult at the free surface" (Crampin, 1985a). The physical reasons for this difficulty are (Crampin, 1984b) that a shear body wave incident upon a free surface at an angle greater than the first critical angle [$\equiv \sin^{-1}(V_s/V_p) \approx 35$ degrees] induces complicated phase and amplitude characteristics in the reflected waves. Even at lesser angles, within the "shear-wave window" where most exploration surface reflection data are acquired, there are mode conversions (SV-P) which complicate the analysis except at normal incidence. Crampin (1985a) notes that "these disturbances are usually much less near vertical incidence ... but even here, shear waves [at the surface] may be disturbed if there are low-velocity layers or any local irregularities..."

A series of papers presented at the 1986 SEG Convention (Thomsen, 1986b; Rai and Hanson, 1986; Lynn and Thomsen, 1986; Alford, 1986b; Willis et al., 1986; and Martin et al., 1986; cf., also Alford, 1986a, and Alford et al., 1986) provided arguments and data to show that these difficulties at the free surface may be overcome by appropriate data acquisition and analysis techniques. Taken as a group, these papers assert that the effects of azimuthal anisotropy on surface shear-wave (S-wave) data are profound and that the implications of the effects are far-reaching. This paper presents the arguments of Thomsen (1986b); the full texts of the other papers will appear in due course.

Some of the conclusions reached herein are very broadly applicable to any uniform azimuthally anisotropic medium (of any symmetry and stemming from any physical cause) and can easily be generalized for vertical layering. However, some of the specific results are valid only for media with a single horizontal axis of rotational symmetry. These employ the equations for transverse isotropy, but with angles measured from the horizontal symmetry axis. Because this is a useful first-order model for discussing azimuthal anisotropy, the casual use of the term "transverse isotropy" to mean, in fact, "vertical transverse isotropy" (Crampin, 1986) is ambiguous. In this paper, media with a vertical axis of rotational symmetry (e.g., shales, thin-bed sequences, etc.) are called "azimuthally isotropic." Use of the term "anisotropy" to mean only this special case, as for example in Thomsen (1986a), should no longer be accepted.

Finally, some of the results below are valid only for that subclass of horizontal transverse isotropy in which the anisotropy is due to a single set of aligned, vertical, circular flat cracks. While preferentially aligned, near-vertical cracks are indeed the most plausible physical cause of azimuthal an-

Presented at the 56th Annual International Meeting, Society of Exploration Geophysicists, 1986. Manuscript received by the Editor January 29, 1987; revised manuscript received August 3, 1987.
*Amoco Production Company, P.O. Box 3385, Tulsa, OK 74102.

isotropy (Crampin, 1985b; Crampin and Atkinson, 1985), most of the present results do not rely on the details of this model. Where the results below have restricted generality, that is indicated at the appropriate place. Nonetheless, it is extremely useful to carry, throughout the discussion, the mental example of aligned vertical cracks and the heuristic analogy (Thomsen, 1986b) of the deck of cards.

As a prelude to attacking realistic problems (involving many layers, structure, etc.), it is first necessary to understand the simplest problem which captures the essence of the issue, i.e., the "canonical" problem. For reflection seismology at the free surface over azimuthally anisotropic media, it is necessary to discuss, at a minimum (1) body-wave propagation in such media, (2) reflection of plane waves at a planar horizontal boundary, and (3) horizontal moveout of reflection arrivals along a receiver spread.

It will develop that, due to the anisotropy, the propagation features (1) and (3) possess anomalies in traveltime which are stable, low-vertical resolution measures of average anisotropy over extended depth intervals, whereas, due to the anisotropy, the reflectivity (2) possesses anomalies in amplitude which are high-resolution measures of local anisotropy differences at the reflecting horizon. Hence, the features are complementary: the traveltime analysis helps one overcome the deleterious effects of azimuthal anisotropy (e.g., it helps one see past the fractures, in order to image the reflectors), whereas the reflection amplitude analysis helps one detect and locate the anisotropy (e.g., it helps one find and characterize locally fractured beds). Therefore, propagation effects (1) and (3) are discussed first, and the reflectivity (2) is discussed subsequently.

BODY-WAVE PROPAGATION IN AZIMUTHALLY ANISOTROPIC MEDIA

Body-wave propagation in azimuthally anisotropic media has been addressed thoroughly by Crampin (1981, 1984a), among others. Nevertheless, it is useful to restate some of these ideas in a form which is less general but more easily visualized and more directly relevant to the canonical problem at hand. In Figure 1 (a map view), the "fracture strike" is a heuristic device only; the discussion immediately following is valid for any azimuthally anisotropic medium. In the general case, the fracture strike direction is the direction of polarization of the "fast" vertically propagating shear mode; cf. Crampin (1984a) and below.

Consider that a conventional *SH* survey is run at an angle oblique to the fracture strike. Since most *S*-wave surveys in the past have been *SH* surveys, oriented without regard to possible azimuthal anisotropy, this is a simple model of past practice. Consider that the vectors shown are polarization (particle-displacement or particle-velocity) vectors corresponding to an impulsive source. Because the medium is assumed to be linear, convolution with a wavelet from a realistic source, or from crosscorrelation of vibrator signal and pilot, may be postponed until later in the analysis. Assume that a conventional stack of a CMP gather forms a trace which is an accurate surrogate for a normal-incidence, multiple-free, noise-reduced trace. Although this assumption is not one to be taken casually, the results of Alford (1986b) and Willis et al. (1986) suggest that it is acceptable in the present context. Hence, the discussion in this section applies only to vertical raypaths; in Figure 1, the rays are normal to the page.

The conventional *SH* survey has a cross-line source polarization and cross-line receivers. The cross-line source is designed to vertically radiate a shear wave with cross-line polarization. However, the equations of wave propagation in an azimuthally anisotropic medium (cf., Crampin, 1984a) assert that such a wave will *not* propagate, even if the medium is only weakly anisotropic. The only shear waves which will propagate vertically in such a medium are those polarized in the principal directions intrinsic to the medium; i.e., parallel to the "fracture strike" and perpendicular to it. (Actually, in the general case, the polarizations are not exactly as just stated, nor are they exactly orthogonal to the propagation direction. However, for weakly anisotropic media, it is acceptable to ignore these complications.) Hence, the source vector, labeled *SH* in Figure 1, is vectorially decomposed by the medium into the two principal components shown, $OS_{||}$ and $OS_{\perp}$, parallel to the principal axes. The decomposition is entirely trigonometric (no physical coupling factors, etc.). It occurs abruptly at the surface of the azimuthally anisotropic medium and does not change with further propagation in the medium, unless the medium itself is vertically inhomogeneous.

Separate shear waves with the two orthogonal polarizations *can* propagate vertically into the medium, each at its own speed. The wave with polarization perpendicular to the cracks can deform the rock easily because of the favorable orientation of the zones of weakness (the cracks). Hence, this wave experiences a low (compliant) effective rigidity, and its velocity $V_{\perp}$ is slow. By contrast, the wave with polarization parallel to the cracks cannot take advantage of the zones of weakness, but must deform the uncracked rock. Hence, this wave experiences a high (stiff) effective rigidity, and its velocity is higher ($V_{||} > V_{\perp}$). The wave with parallel polarization advances faster than the wave with perpendicular polarization, as each propagates vertically. This is shear-wave splitting (Crampin, 1985a), a manifestation of the anisotropy.

It is useful to recall that elastic anisotropy means a dependence of elastic wave speed upon direction. The direction may be taken as either direction of propagation or direction of polarization. Each velocity (V_p, $V_{||}$, $V_{\perp}$) varies smoothly with the direction of propagation. By contrast, the variation of shear velocity with the direction of polarization is discrete: for a given direction of propagation, only two orthogonal polarizations will propagate. Intermediate polarizations decompose vectorially into these principal components.

If the shear-wave signal were a continuous sinusoid rather than an impulse, the interference between these two modes would yield an apparent single sinusoidal signal with elliptical polarization. That is, the shear wave would appear to twist in its polarization (like a corkscrew) as it advanced. However, the seismic wavelet is not a continuous sinusoid but is localized in time. If it were a perfect spike, then each pure mode would also propagate as a spike, linearly polarized in the appropriate direction, and no elliptical polarization would be apparent. Instead, the signal would appear as two separated impulsive events. In the actual case of imperfect localization, the effects will be intermediate between these extreme cases.

Returning to Figure 1, the two shear phases propagate vertically down and reflect independently from the horizontal reflector, with corresponding reflection coefficients $R_{||}$ and $R_{\perp}$. If the anisotropy is very weak, and/or similar in the incident and reflecting media, then the two reflection coefficients will be similar. Furthermore, in the weak anisotropy case, the geometric spreading, attenuation, etc. will be similar for the two

modes. This is a common circumstance, as demonstrated by the data of Willis et al. (1986); the exceptional case is discussed in the final section. In the common case, the largest difference in amplitude between the two returning waves will be due to the trigonometric factors discussed here. For clarification of these geometrical effects, the physical factors are ignored in Figures 1 and 2, i.e., the amplitudes of the polarization vectors of the returning wave are then identical to the respective components of the source vector. However, the physical factors are retained in the mathematical development below.

The receivers are, by convention, oriented cross-line and hence detect not the entire reflected wave, but only the cross-line component of each mode. Hence, the fast (∥) mode arrives with an amplitude, as measured on the cross-line receiver (cf., Figure 2a), of

$$R_{\parallel} \sin^2 \theta f_{\parallel}(t) * \delta\left(t - \frac{2z}{V_{\parallel}}\right),$$

where $f_{\parallel}(t)$ is a filter embodying geometric spreading, attenuation, etc. and the delayed Dirac (δ) indicates a spike arriving from depth z with velocity $V_{\parallel}$.

A split second later, the slow mode ($\perp$) arrives, with apparent amplitude on the cross-line receiver (cf., Figure 2a) of

$$R_{\perp} \cos^2 \theta \, f_{\perp}(t) * \delta\left(t - \frac{2z}{V_{\perp}}\right).$$

Hence, the receiver will detect two arrivals from a single reflector rather than one arrival. The separation in time will be

$$\Delta t \equiv t_{\perp} - t_{\parallel} = t_{\parallel}\left(\frac{t_{\perp}}{t_{\parallel}} - 1\right)$$

$$= t_{\parallel}\left[\left(\frac{2z}{V_{\perp}}\Big/\frac{2z}{V_{\parallel}}\right) - 1\right] = t_{\parallel}\left(\frac{V_{\parallel}}{V_{\perp}} - 1\right) = \gamma t_{\parallel}. \qquad (1)$$

The anisotropy,

$$\gamma \equiv \left(\frac{V_{\parallel}}{V_{\perp}} - 1\right) \approx \left(1 - \frac{V_{\perp}}{V_{\parallel}}\right), \qquad (1a)$$

corresponds, in the special case of horizontal transverse isotropy, to the anisotropy parameter γ defined by Thomsen (1986a).

A wavelet $w(t)$ of finite duration, convolved with the above impulse sequence, will yield the following signal on the cross-

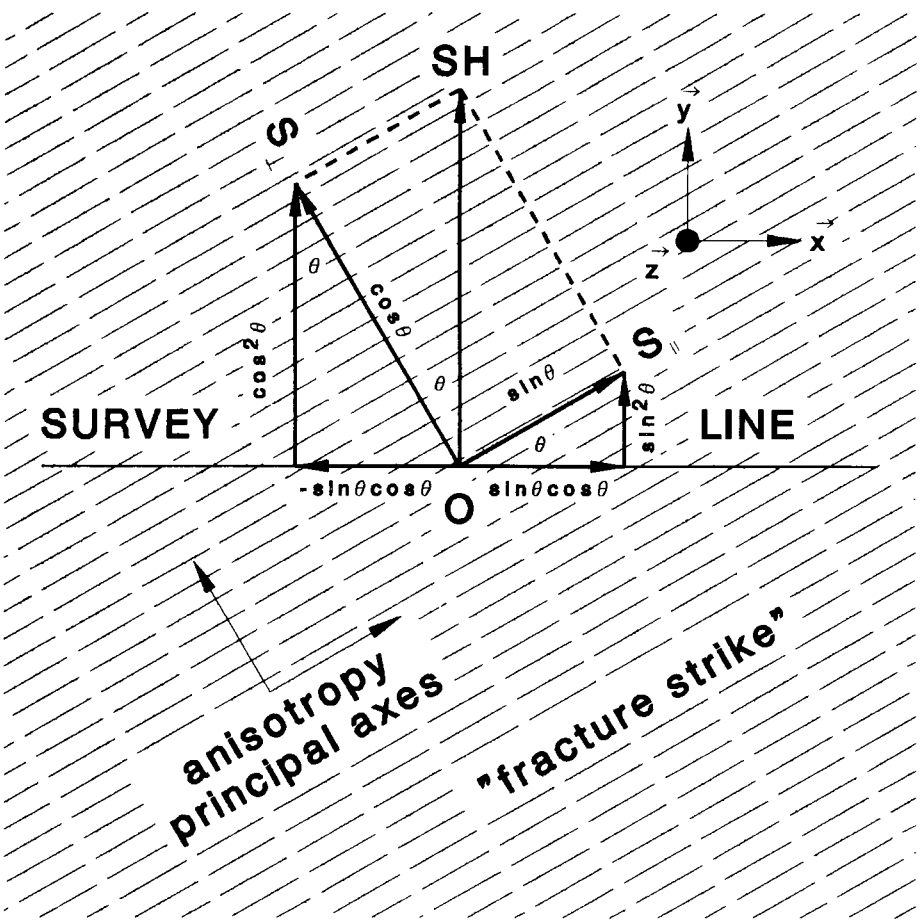

FIG. 1. Map view of the canonical reflection problem for an *SH*-wave survey oblique to the anisotropy.

line receiver:

$$s_{22}(t) = \Big[R_{\|} \sin^2 \theta \, \delta(t - t_{\|}) * f_{\|}(t) + R_{\perp} \cos^2 \theta \, \delta(t - t_{\perp}) * f_{\perp}(t) \Big] * w(t). \quad (2)$$

Here, the first subscript 2 on s indicates a cross-line (y) receiver; the second subscript 2 on s indicates a cross-line source.

If the duration of the wavelet is comparable to the delay Δt, there will be complicated interference between the two arrivals, which may substantially degrade the apparent quality of the data. This will happen even if the anisotropy is small, since the time delay [equation (1)] depends upon the traveltime itself. For example, if $\gamma \approx 2$ percent, then at long times ($t_{\|} > 2$ s) the time delay will be $\Delta t > 40$ ms, i.e., will be comparable to the duration of the main lobe of a typical wavelet. Alford (1986b) analyzed this effect and suggested that it is a principal cause of erratic and unpredictable S-wave data quality worldwide. Alford's conclusion was confirmed by Willis et al. (1986). Also, Rai and Hanson (1986) confirmed this analysis in a well-controlled laboratory context.

If in-line receivers are also deployed, then the rest of the signal may be recovered. Figure 1 also shows the trigonometric factors which decompose the returning signal into the in-line direction. Again, two arrivals are recorded, with equal and opposite amplitudes, separated by the same time delay as the cross-line arrivals (Figure 2b):

$$s_{12}(t) = \Big[R_{\|} \sin \theta \cos \theta \, \delta(t - t_{\|}) * f_{\|}(t) - R_{\perp} \sin \theta \cos \theta \, \delta(t - t_{\perp}) * f_{\perp}(t) \Big] * w(t). \quad (3)$$

Recall that, in a survey over flat-lying isotropic media with a cross-line source, the in-line receiver records a null trace. This isotropic result may be recovered from the present anisotropic analysis by realizing that, in the isotropic limit ($\gamma = 0$), the time delay vanishes and the reflectivities and propagation filters are identical so that the two in-line arrivals exactly cancel each other. In this same limit, the cross-line signal (2) also reduces to the isotropic result, since [cf., equation (2)]

$$\sin^2 \theta + \cos^2 \theta = 1.$$

A nonzero in-line signal from a cross-line survey in flat-lying geometry is a sensitive detector of even very weak azimuthal

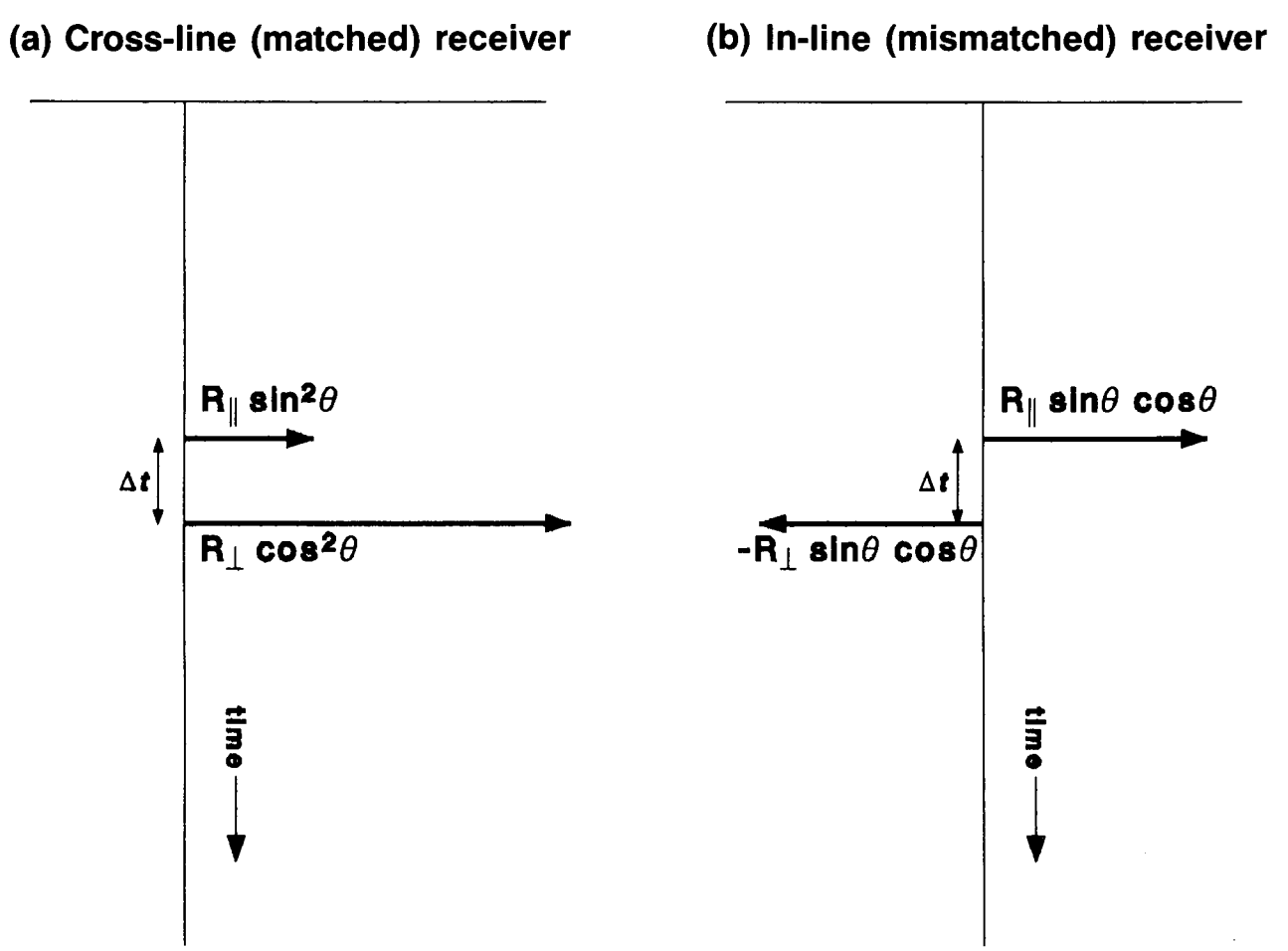

FIG. 2. Apparent reflection spike series for the canonical reflection problem of Figure 1. One reflector yields two spikes on both (a) the cross-line receiver and (b) the in-line receiver.

anisotropy (Alford, 1986b). Both shear modes propagate through the same rock, so that small differences in their arrival times can be easily detected, in a relative sense, as in an interferometer. Velocity differences of 1–3 percent have a substantial deleterious effect on the data and may be measured quantitatively (see below) even though the uncertainty in either of the absolute velocities may be much higher than 1–3 percent. By contrast, *P*-wave anisotropy in azimuthally isotropic media must be determined by comparison of traveltimes over different raypaths (vertical and oblique), wherein refractive ray bending causes effects of comparable size. Hence, *P*-wave anisotropy in azimuthally isotropic media is not susceptible to such sensitive detection techniques.

It is easy to see that if a conventional *SV* survey (with an in-line source and receiver) were run over the same line, there would be similar splitting effects, although with different trigonometric relationships. The in-line and cross-line components, respectively, yield signals

$$s_{11}(t) = \Big[R_{||} \cos^2\theta\ \delta(t - t_{||}) * f_{||}(t) + R_{\perp} \sin^2\theta\ \delta(t - t_{\perp}) * f_{\perp}(t) \Big] * w(t); \tag{4}$$

and

$$s_{21}(t) = \Big[R_{||} \sin\theta \cos\theta\ \delta(t - t_{||}) * f_{||}(t) - R_{\perp} \sin\theta \cos\theta\ \delta(t - t_{\perp}) * f_{\perp}(t) \Big] * w(t). \tag{5}$$

These results may easily be generalized to the multilayer case, if the principal directions in each of the layers are oriented the same. In this case, there is no further splitting at deeper horizons of the two transmitted shear modes, and *each* reflector is represented in the data by two pulses. The variable degree of anisotropy within each layer is encoded in the time separation of corresponding reflection events. Equations (2)–(5) may be generalized to treat this case with the replacements

$$R_{||}\,\delta(t - t_{||}) \rightarrow r_{||}(t)$$

and

$$R_{\perp}\,\delta(t - t_{\perp}) \rightarrow r_{\perp}(t),$$

where $r_{||}(t)$ and $r_{\perp}(t)$ are the principal reflectivity series (one spike per reflector, ignoring multiples) corresponding to the fast and the slow modes, respectively. By the previous arguments, one expects $r_{\perp}(t)$ to be, to a good approximation, just a stretched and scaled version of $r_{||}(t)$. The stretching factor γ will, in general, be time-variant. The time delay between corresponding reflectors is, generalizing equation (1),

$$\Delta t(t_{||}) = \bar{\gamma}(t_{||}) t_{||}, \tag{6}$$

where $\bar{\gamma}(t_{||})$ is the average value of anisotropy from $t = 0$ down to $t = t_{||}$. Local values of anisotropy, denoted by $\gamma(t_{||})$ without the bar, may in principle be determined by an appropriate differentiation of $\bar{\gamma}(t_{||})$; but in practice the procedure may not be very stable.

If different layers possess different orientations of anisotropy, then in general each mode will split again at each such interface and each reflector will be represented in the data by many reflection spikes. Repeated splitting does not appear to be a common circumstance, given the success (Willis et al., 1986) of the simple model above. This apparent uniformity of orientation of anisotropy, independent of depth, is readily justified (e.g., Crampin and Atkinson, 1985), since preferential crack alignments are controlled by preferential stress alignments and the stress direction is uniform on a regional basis and uniform in depth, except within areas of intense tectonic deformation.

An important exception to the previous argument exists, which is contradicted by neither the seismic data (Willis et al., 1986) nor the physical argument (e.g., Crampin and Atkinson, 1985). This exception is the possibility of beds which retain, even in the current stress regime, cracks created by a paleostress with different orientation that remain open despite the current unfavorable stress through an exceptional mechanism. An example of such an occurrence is reported by Lynn and Thomsen (1986); the exceptional mechanism was partial precipitation of quartz in the cracks while they were held open by a previous stress regime, so that subsequent evolution of the stress field could not close the cracks.

If the bed with exceptional orientation of anisotropy is thin, then each of the reflection spikes in $r_{||}(t)$ and $r_{\perp}(t)$ is replaced by a quadruplet of closely spaced spikes corresponding to additional splitting of each mode on transmission each way through the exceptional bed. However, if the product (thickness times anisotropy) of the exceptional bed is sufficiently small, then the quadruplet will be blurred by convolution with the wavelet, and the splitting will not be detectable with traveltime methods. If the product is not small, then that fact will be revealed by failure of the algorithm defined below.

DETERMINATION OF THE PRINCIPAL TIME SERIES

Crampin (e.g., 1985b) has emphasized the utility of polarization diagrams in the analysis of these split shear arrivals. While such diagrams undoubtedly lead to important insights, the details of the polarization trajectories do depend strongly upon the shapes and relative amplitudes of the two wavelets and the delay between the two pulses. Further, the study of polarization diagrams lends itself most easily to the detailed investigation of particular events, rather than to summary investigations of entire seismic sections.

The analysis technique of Alford (1986b) offers a complementary set of advantages and disadvantages. Here a different derivation of that algorithm is presented, based upon the simple model above. The problem is to derive from the data $s_{ji}(t)$, which contain two events per reflector, the "principal time series"

$$s_{||}(t_{||}) = f_{||} * w * r_{||}$$

and

$$s_{\perp}(t_{\perp}) = f_{\perp} * w * r_{\perp},$$

containing one event per reflector. Both $s_{||}$ and $s_{\perp}$ should be easier to interpret than the original data, since each is free of the interference between the two principal modes of *S*-wave propagation. Furthermore, the *difference* between corresponding events on $s_{||}(t_{||})$ and $s_{\perp}(t_{\perp})$ contains information about azimuthal anisotropy which is confounded in the original data.

Given a complete data set (cross-line source and in-line source, both into cross-line and in-line receivers), the solution

of equations (2)–(5) is straightforward:

$$s_{||}(t) = \cos^2\theta\, s_{11}(t) + \sin\theta\cos\theta\left[s_{21}(t) + s_{12}(t)\right] + \sin^2\theta\, s_{22}(t); \quad (7a)$$

$$s_{\perp}(t) = \sin^2\theta\, s_{11}(t) - \sin\theta\cos\theta\left[s_{21}(t) + s_{12}(t)\right] + \cos^2\theta\, s_{22}(t). \quad (7b)$$

The same analysis produces two complementary equations:

$$0 = \sin^2\theta\, s_{21}(t) + \sin\theta\cos\theta\left[s_{11}(t) - s_{22}(t)\right] - \cos^2\theta\, s_{12}(t); \quad (8a)$$

$$0 = \sin^2\theta\, s_{12}(t) + \sin\theta\cos\theta\left[s_{11}(t) - s_{22}(t)\right] - \cos^2\theta\, s_{21}(t). \quad (8b)$$

Alford (1986b) derived the results of equations (7) and (8) from a different point of view. Examination of equations (8) shows that both equations cannot be satisfied unless the original data on the mismatched receivers are identical, i.e.,

$$s_{12}(t) = s_{21}(t). \quad (9)$$

Although equation (9) is trivially satisfied by the model, it is not necessarily satisfied by the data and constitutes a useful quality control; unless equation (9) is satisfied by the data to acceptable precision, the model-driven processing (7) is not justified.

If equation (9) is satisfied, equations (8a) and (8b) are identical and constitute a determination of the unknown orientation angle θ (Alford, 1986b). In practice (Willis et al., 1986), equations (7a), (7b), (8a), and (8b) are calculated for a sequence of values of θ; the value chosen for θ is that for which the linear combination of data on the right-hand side of equation (8) is approximately zero at all times for a suite of adjacent CMP points. This angle θ then defines the weights for linearly combining the data $s_{ji}(t)$ into the principal time series $s_{||}(t)$ and $s_{\perp}(t)$, as in equation (7).

If the complete suite of seismograms s_{11}, s_{21}, s_{22}, s_{12} is not available, the principal time series may still be recovered, albeit less robustly. If the orientation angle θ is known, any two of equations (2)–(5) may be used to calculate the two unknowns $s_{||}(t)$ and $s_{\perp}(t)$. If θ is not known a priori, a procedure similar to that outlined above may be implemented: solving any two of equations (2)–(5) with several values of fixed θ we choose that solution for which the resulting $s_{\perp}(t)$ looks like a stretched version of $s_{||}(t)$ at all times and for a suite of adjacent CMP points. For example, given a conventional cross-line source and both cross-line and in-line receivers, the solution [from equations (2) and (3)] is

$$s_{||}(t) = s_{22}(t) + \cot\theta\, s_{12}(t) \quad (10a)$$

and

$$s_{\perp}(t) = s_{22}(t) - \tan\theta\, s_{12}(t). \quad (10b)$$

Equations (10) represent just a rotation of the data, followed by an angle-dependent scaling. If $\theta = 0$ or $\theta = \pi/2$ in some particular case, equations (10) are unstable. However, this case will be self-evident, since the mismatched receiver will record only noise. This method [single-source multiple receivers, equations (10)] was used by Martin et al. (1986).

By use of equations (7) or equations (10) on each set of traces along a survey line, the partial redundancy of conventionally acquired surface reflection data is used to overcome the problems (Crampin, 1984b, 1985a) which are potentially associated with surface data.

NORMAL AND ABNORMAL MOVEOUT

It is well-known in the context of azimuthal isotropy that the horizontal moveout of reflected energy from flat-lying geometry is abnormal. That is, the moveout velocity is not equal to the vertical velocity, even in the one-layer case. Intuition suggests that, in the present case of azimuthal anisotropy, the moveout may also be abnormal. To simplify this discussion, only two special cases are considered here, corresponding to survey lines parallel to one or the other principal directions of anisotropy. At other azimuths, the waves are split and the situation is much more complex.

The abnormality of moveout clearly depends upon the angular variation of velocity. Hence, in this section it is not possible to maintain the generality of the previous section; the following results are restricted to the case of horizontal transverse isotropy. The results are cast in terms of the three measures of anisotropy (ε, δ, γ) defined by Thomsen (1986a) and are restricted to the case of weak anisotropy. Under these assumptions, the departures of the rays from the sagittal plane may be neglected (Backus, 1965).

First consider a survey line running parallel to the strike of the symmetry planes of the medium, i.e., parallel to the fracture strike of Figure 1. Since by assumption all directions of propagation in this plane are equivalent, there is no angular variation of velocity and moveout is normal. That is, moveout velocity is identical to vertical velocity for each type of survey: *P*, *SV*, and *SH*. (Of course, the vertical velocity for the *SV* survey is faster than that of the *SH* survey, as discussed in the section on body-wave propagation.)

Consider next a survey line running perpendicular to the strike of the symmetry planes, i.e., perpendicular to the fracture strike of Figure 1. The moveout is nonhyperbolic and, in general, its description requires more than one parameter. To simplify the discussion, only the short-spread limit is considered here; the moveout velocity is defined by

$$V_{mo}^2 \equiv \lim_{x\to 0}\left[\frac{d(x^2)}{d(t^2)}\right], \quad (11)$$

for each wave type, where x is offset and t is arrival time.

Modifying the arguments of Thomsen (1986a) to this geometry, it is easy to show that

for a *P*-wave survey,

$$V_{mo}(P) = V_{P_0}(1 - \delta); \quad (12a)$$

for an *SV*-wave survey,

$$V_{mo}(SV) = V_{||}\left[1 - \gamma + (V_{P_0}/V_{||})^2(\varepsilon - \delta)\right]; \quad (12b)$$

for an *SH*-wave survey:

$$V_{mo}(SH) = V_{\perp} = V_{||}(1 - \gamma). \quad (12c)$$

In these expressions, V_{P_0} is the vertical P-wave velocity; in the special case where the anisotropy is caused by vertically aligned cracks, V_{P_0} is also the intrinsic velocity of the uncracked rock. $V_{||}$ and $V_{\perp}$ are the vertical shear speeds for polarization along the principal directions, as in the previous section. In the special case of vertical aligned cracks, $V_{||}$ is the intrinsic shear velocity of the uncracked rock.

ε, δ, and γ are nondimensional measures of anisotropy, defined by Thomsen (1986a), which reduce to small numbers in the limit of weak anisotropy and which were chosen to simplify equations such as these. In general, these are all independent numbers, but in the special case of aligned vertical cracks, they are all dependent upon the crack density. Since δ and ε are independent numbers, it can happen for some anisotropic media that $\delta < \varepsilon$. In fact, for the special case of anisotropy due to aligned vertical cracks, this is indeed the case. For this special case one can show that the combination

$$\frac{V_{P_0}^2}{V_{||}^2}(\varepsilon - \delta) \approx \gamma \tag{13}$$

for plausible values of the underlying parameters. Hence, in this case equations (12b) and (12c) yield

$$V_{mo}(SV) \approx V_{||}; \tag{14}$$

and equations (12b) and (12c) may be arranged to show the inequality

$$V_{mo}(SH) = V_{\perp} < V_{mo}(SV) \approx V_{||}. \tag{15}$$

This inequality sequence for moveout velocities may be contrasted with the corresponding sequence for the vertical velocities of the two shear modes. For the present orientation of the survey line with respect to anisotropy, the vertical velocities are

for a P-wave survey,

$$V_{vert}(P) = V_{P_0}, \tag{16a}$$

for an SV-wave survey,

$$V_{vert}(SV) = V_{\perp}, \tag{16b}$$

and

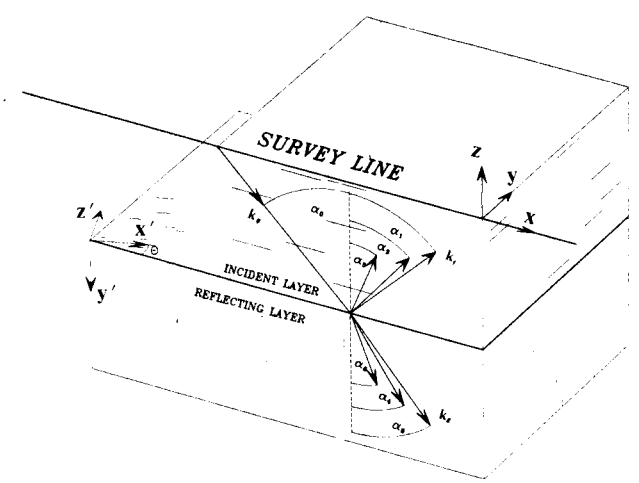

FIG. 3. 3-D cross-section of the canonical reflection problem showing vertical variation in anisotropy.

for an SH-wave survey,

$$V_{vert}(SH) = V_{||}, \tag{16c}$$

yielding an inequality sequence

$$V_{vert}(SV) = V_{\perp} < V_{vert}(SH) = V_{||}. \tag{17}$$

Comparison of the sequences (15) and (17) shows that the order of velocities is reversed; for moveout velocities, the SH-wave survey is slower; while for the vertical velocities, the SV-wave survey is slower. The SV reflection comes in later (at vertical incidence) but moves out faster.

These results are always true if the anisotropy is due to a single set of vertically aligned cracks which is adequately modeled by the theory. For more general situations, with many layers and/or with vertical transverse isotropy, the results may not be true but are always plausible.

REFLECTIVITY

Consider now the problem of reflection of plane waves at the planar boundary between two anisotropic media. This problem was treated in great generality by Keith and Crampin (1977). Since then, quite general modeling codes for wave propagation in azimuthally anisotropic media have become available (Crampin et al., 1986, Gajewski and Psencik, 1988). Nonetheless, in order to expose the critical ideas, it is useful to sketch the development of a less general theory, which still contains the essence of the problem. Consider the problem illustrated in Figure 3, of a plane wave incident upon a planar boundary between two transversely isotropic media. In the example, the upper medium (e.g., a shale) has a vertical symmetry axis; the lower medium (e.g., a sandstone permeated with vertical aligned cracks) has a horizontal symmetry axis running at an oblique angle to the line of survey.

In either medium, the wave equation has three plane-wave solutions, one quasi-longitudinal, one transverse, and one quasi-transverse. The solutions are given, for example, by Daley and Hron (1977), whose notation is followed here. The index ν is used to distinguish the various waves:

$\nu = 0$ incident wave (P, $S_{||}$, or $S_{\perp}$);

$\nu = 1$ reflected P-wave;

$\nu = 2$ transmitted P-wave;

$\nu = 3$ reflected $S_{\perp}$-wave;

$\nu = 4$ transmitted $S_{\perp}$-wave;

$\nu = 5$ reflected $S_{||}$-wave;

$\nu = 6$ transmitted $S_{||}$-wave;

so that even values for ν indicate a downgoing wave, odd values for ν indicate an upgoing wave.

All of the difficulties in the reflection-transmission mode-conversion problem are geometric. The waves are easily expressed in the natural (intrinsic) coordinate frame of each medium, whereas the boundary conditions (which determine the energy partition) are easily expressed in the survey-interface coordinate frame. This conflict does not arise in dealing with isotropic media.

In Figure 3, the intrinsic coordinate frame (primed) of the lower medium is related to the survey frame (unprimed) by

two sequential rotations: a clockwise rotation by θ about $\mathbf{y}'$, followed by a clockwise rotation by $\pi/2$ about the new $\mathbf{x}$. The corresponding rotation matrix is

$$\mathbf{\Omega} = \begin{bmatrix} 1 & 0 & 0 \\ 0 & 0 & 1 \\ 0 & -1 & 0 \end{bmatrix} \begin{bmatrix} \cos\theta & 0 & -\sin\theta \\ 0 & 1 & 0 \\ \sin\theta & 0 & \cos\theta \end{bmatrix}$$

$$= \begin{bmatrix} \cos\theta & 0 & -\sin\theta \\ \sin\theta & 0 & \cos\theta \\ 0 & -1 & 0 \end{bmatrix} . \tag{18}$$

Any vector $\mathbf{g}'$ expressed in the primed frame may be transformed to the unprimed frame through operation by $\mathbf{\Omega}$:

$$\mathbf{g} = \mathbf{\Omega}\mathbf{g}'. \tag{19}$$

Similarly, a tensor expressed in the primed frame may be transformed to the unprimed frame using $\mathbf{\Omega}$. For example, in the primed frame the intrinsic elastic modulus tensor $\mathbf{C}^{(2')}$ of the medium has the simple form of the hexagonal symmetry class (cf., e.g., Nye, 1957; Thomsen, 1986a). However, in the survey frame, $\mathbf{C}^{(2)}$ is

$$\mathbf{C}^{(2)} = \mathbf{\Omega}^T\mathbf{\Omega}^T\mathbf{C}^{(2')}\mathbf{\Omega}\mathbf{\Omega}, \tag{20a}$$

where T indicates the transpose. In expanded notation, equation (20a) is written as

$$C^{(2)}_{ijkl} = C^{(2')}_{mnpq}\Omega_{mi}\Omega_{nj}\Omega_{pk}\Omega_{q\ell}, \tag{20b}$$

with summation over repeated indices. $\mathbf{C}^{(2)}$ has nonzero components $C^{(2)}_{3312}$ and $C^{(2)}_{2313}$ and other effects of the rotational mixing. (Use of the matrix $C_{\alpha\beta}$ in place of the tensor $C_{ijk\ell}$ may lead the unwary into error.)

To complicate matters, any other coordinate frame related to the primed system by a rotation about the symmetry axis ($\mathbf{z}'$) is also a valid intrinsic coordination system for this (transversely isotropic) lower medium (Figure 4). Any vector $\mathbf{g}''$ expressed in such a system may be transformed to the primed system by a rotation about the symmetry axis by an arbitrary angle β:

$$\mathbf{g}' = \begin{bmatrix} \cos\beta & \sin\beta & 0 \\ -\sin\beta & \cos\beta & 0 \\ 0 & 0 & 1 \end{bmatrix} \mathbf{g}''. \tag{21}$$

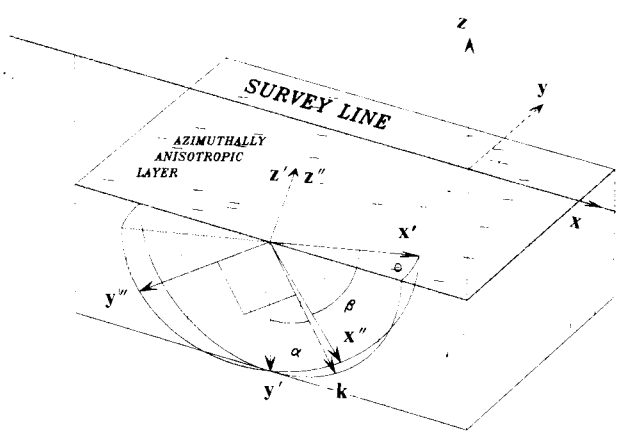

FIG. 4. Detail of Figure 3 showing expanded relationship of coordinate frames.

The most conventient such frame is defined so that the $\mathbf{y}''$ axis, while remaining in the invariant ($\mathbf{x}' - \mathbf{y}'$) plane, is perpendicular to the wave vector $\mathbf{k}$, which lies in the survey ($\mathbf{x} - \mathbf{z}$) plane. In this frame, the polarization eigenvector $\mathbf{g}''_6$ for the transmitted $S_{||}$ mode is trivial:

$$\mathbf{g}''_6 = \mathbf{y}'' = (0, 1, 0). \tag{22}$$

This eigenvector is transformed to the primed frame with equation (21),

$$\mathbf{g}'_6 = (\sin\beta_6, \cos\beta_6, 0),$$

and to the survey frame with equation (19),

$$\mathbf{g}_6 = (\cos\theta\sin\beta_6, \sin\theta\sin\beta_6, -\cos\beta_6).$$

The orthogonality condition, $\mathbf{g}_6 \cdot \mathbf{k}_6 = 0$, then determines the required angle β_6 in terms of the incidence angle α_6 and the orientation θ of the survey line:

$$\cot\beta_6 = -\tan\alpha_6\cos\theta. \tag{23}$$

Similar arguments define the transformed eigenvectors $\mathbf{g}_4$ and $\mathbf{g}_2$ of the other two modes in the survey coordinate frame.

With this notation, the rest is straightforward. The boundary conditions are continuity of three components of displacement and continuity of three components of stress at $z = 0$. The displacement boundary conditions may be written together as

$$\sum_{\nu=1}^{6}(-1)^\nu\mathbf{u}_\nu = \mathbf{u}_0, \tag{24}$$

where the $\mathbf{u}_\nu$ are the plane-wave displacements from Daley and Hron (1979), with the obvious typographical errors corrected. The factors $(-1)^\nu$ bring all outgoing waves to the left side of the equation. Of course, the solutions for $\nu = 2, 4, 6$ must be transformed into the survey coordinate frame using equations (23), (21), and (19).

The stress boundary conditions may be written together as

$$\sum_{\nu=1}^{6}(-1)^\nu\sigma_{i3}(\mathbf{u}_\nu) = \sigma_{i3}(\mathbf{u}_0), \qquad i = 1, 2, 3, \tag{25}$$

where $\sigma_{i3}(\mathbf{u}_\nu)$ is a component of stress due to the ν^{th} mode:

$$\sigma_{i3}(\mathbf{u}_\nu) = \tfrac{1}{2}C^{(\nu)}_{i3k\ell}\left(\frac{\partial u_k}{\partial x_\ell} + \frac{\partial u_\ell}{\partial x_k}\right)_\nu . \tag{26}$$

The subscript 3 selects those components of stress applied on the interface plane ($z = x_3 = 0$). Of course, $\mathbf{C}^{(2)} = \mathbf{C}^{(4)} = \mathbf{C}^{(6)}$ is the elasticity tensor (20) of the lower medium, expressed in the survey frame.

The six equations (24) and (25) constitute six equations in six unknowns, the amplitudes of the six outgoing waves, normalized to U_0. Because of the nonzero values of $C^{(2)}_{3312}$ and $C^{(2)}_{2313}$, in general all six are coupled together. As in the isotropic case, no solution is possible unless all frequencies are equal or unless all horizontal wavenumbers are equal. This last requirement determines the incidence (departure) angles α_ν through a generalized Snell's law:

$$\frac{\sin\alpha_0}{V_0(\alpha_0)} = p = \frac{\sin\alpha_\nu}{V_\nu(\alpha_\nu)}, \qquad \nu = 1, \ldots, 6, \tag{27}$$

where p is the "wavefront parameter." The phase velocities V_ν with their angular dependence are given by Daley and Hron (1979).

The six linear equations in six unknowns possess a solution for which the $\hat{y}$ component of each wave vector $\mathbf{k}$ is zero, i.e., all wave vectors lie exactly in the sagittal plane. Therefore, by the uniqueness theorem, this solution is the only one. The energy-flux vector departs from this plane in general (cf., Thomsen, 1986a and prior discussion), but for weak anisotropy, the effect is small.

The solution to the six equations is algebraically cumbersome and is best left implicit. Figure 5 illustrates numerical results for incident *P*-waves and *SH*-waves at various incidence angles with parameters appropriate to the case of Lynn and Thomsen (1986). For *P*-wave reflectivity, there is, of course, no azimuthal dependence at normal incidence, and only modest azimuthal dependence at oblique incidence. This result verifies the common experience that *P*-wave amplitudes of stacked traces at the tie points of crossing survey lines are independent of azimuth, even though most sedimentary sections are azimuthally anisotropic (Willis et al., 1986).

By contrast, the *SH* reflectivity (cross-line source, cross-line receiver) shows a strong azimuthal dependence at all angles of incidence. This azimuthal variation will remain evident in the stacked traces, making a clear diagnosis of the presence of azimuthal anisotropy at the reflecting horizon. The nature of this dependence is clarified by examination of the special case of the solutions to equations (24) and (25) corresponding to a normally incident *SH*-wave polarized along one or the other principal axes of anisotropy. For the case where the survey line is perpendicular to the cracks, the normal-incidence *SH* reflectivity from equations (24) and (25) reduces to a familiar form

$$R_{SH}(\theta = \pi/2) = -\frac{\rho_2 V_{\|_2} - \rho_1 V_{S1}}{\rho_2 V_{\|_2} + \rho_1 V_{S1}}, \tag{28}$$

where V_{S1} is the vertical shear velocity in the upper medium. [Note the minus sign on the right side of equation (28). This sign convention is described and justified by Aki and Richards (1980). The present results reduce to theirs in the isotropic limit.]

For the case where the survey line is parallel to the cracks, the normal-incidence *SH* reflectivity is

$$R_{SH}(\theta = 0) = \frac{\rho_2 V_{\perp 2} - \rho_1 V_{S1}}{\rho_2 V_{\perp 2} + \rho_1 V_{S1}} \tag{29a}$$

$$= -\frac{\rho_2 V_{\|_2}(1 - \gamma_2) - \rho_1 V_{S1}}{\rho_2 V_{\|_2}(1 - \gamma_2) + \rho_1 V_{S1}}. \tag{29b}$$

If the difference in shear impedance is small, equation (29) becomes

$$R_{SH}(\theta = 0) \approx R_{SH}(\theta = \pi/2) + \tfrac{1}{2}\gamma_2. \tag{29c}$$

Of course at normal incidence, an *SV* (in-line) source has a reflectivity

$$R_{SV}(\theta) = R_{SH}(\pi/2 - \theta),$$

so that equation (29c) becomes

$$R_{SH}(\theta = 0) = R_{SV}(\theta = 0) + \tfrac{1}{2}\gamma_2. \tag{30}$$

It is clear that if the upper medium is also azimuthally anisotropic with its principal axes oriented in the same direction as those of the lower medium, then equations (28) and (29a) may be straightforwardly generalized by replacing V_{S1} by $V_{\|_1}$ or $V_{\perp 1}$ as appropriate. Then equations (29c) and (30) became

$$R_{SH}(\theta = 0) = R_{SH}(\theta = \pi/2) + \tfrac{1}{2}(\gamma_2 - \gamma_1) \tag{31a}$$

$$= R_{SV}(\theta = 0) + \tfrac{1}{2}(\gamma_2 - \gamma_1). \tag{31b}$$

In this case intermediate orientations of the survey line will produce shear-wave splitting. The present analysis then applies to the principal reflectivity series $r_{\|}(t)$ and $r_{\perp}(t)$, so that equation (31b) generalizes to

$$r_{\perp}(t_{\perp}) = r_{\|}(t_{\|}) + \tfrac{1}{2}(\gamma_2 - \gamma_1). \tag{31c}$$

It is clear from equations (31) that if a sequence of azimuthally anisotropic layers (with axes oriented alike) has differing parallel shear impedance in each layer but identical anisotropy [$\gamma(z) = \gamma_1 = \gamma_2$ for all z], then the reflectivity will *not* show azimuthal variation. Consequently, the principal time series $s_{\|}(t)$ and $s_{\perp}(t)$ will show comparable reflection amplitudes. $s_{\perp}(t)$ will appear as a stretched, unscaled version of $s_{\|}(t)$.

If $\gamma(z)$ is a smooth function of z, this last statement will be almost true. This is a common situation, as shown by the relative similarity of $s_{\|}(t)$ and $s_{\perp}(t)$ in many areas (cf., Alford, 1986b, and Willis et al., 1986).

Even given this generality, there will be certain reflecting horizons where $\gamma_2 \neq \gamma_1$ and where the principal time series show a definite difference in amplitude. Locally, $s_{\perp}(t)$ will be scaled, as well as stretched, relative to $s_{\|}(t)$. Such a case constitutes a detection with high vertical resolution of a difference in *local* anisotropy, $\gamma_2 - \gamma_1$. If the anisotropy is due to near-vertical aligned cracks or joints (the most plausible physical cause, cf., Crampin and Atkinson, 1985), this difference between $s_{\perp}(t)$ and $s_{\|}(t)$ constitutes a detection from the surface, with high vertical resolution, of intensely fractured beds at depth.

This sort of detection was reported by Lynn and Thomsen (1986). In that case, the orientation of the cracks in the intensely cracked beds also differed from the orientation of cracks in the overlying beds, but the principle is the same as in the present, simpler analysis.

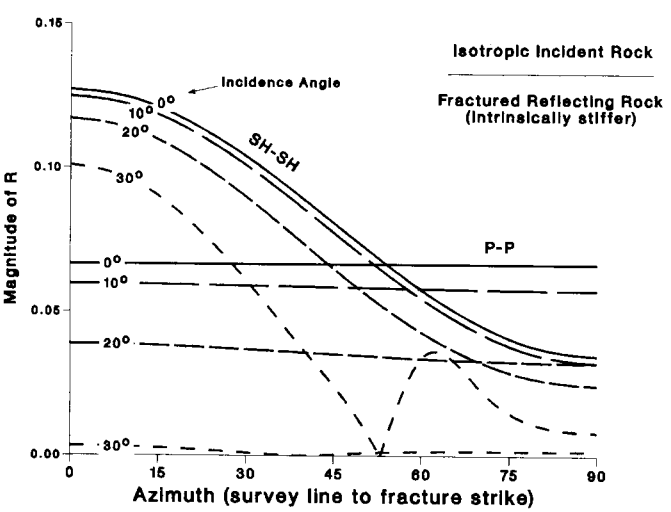

FIG. 5. Numerical example of reflection coefficients as functions of azimuth and incidence angle.

SUMMARY

This discussion, in conjunction with previous work by Crampin and his coauthors and by Alford, Lynn, Rai, Hanson, Willis, Rethford, and Bielanski, has established that

(1) Shear waves traveling nearly vertically in azimuthally anisotropic media are noticeably affected by such anisotropy, even when the anisotropy is very weak.

(2) The effects are visible in conventionally acquired surface *S*-wave data taken in typical exploration contexts; the massive redundancy of conventional acquisition techniques with closely spaced CMP gathers overcomes the difficulties potentially caused by the free surface.

(3) Because *S*-waves of both polarizations travel through very nearly the same body of rock but at different velocities, a proper comparison of multiple-component records can reliably reveal very small velocity differences, as in an interferometer.

(4) The anisotropy becomes noticeable in the data at record times such that the ratio of the wavelet duration to the traveltime becomes comparable to the anisotropy, e.g., γ as small as 1 percent may be detected. Anisotropy may seriously degrade apparent record quality, unless properly corrected for.

(5) Resolution of raw data into the two principal time series allows one to remove the interference between the two shear modes, and, by seeing past the fractures, to image the reflectors. This operation also determines the orientation of the anisotropic axes, and hence, with additional assumptions, the orientation of the fractures and the principal stresses.

(6) The time difference between corresponding events on the two principal time series provides a robust measure, poorly resolved in time, of average anisotropy over extended depth intervals.

(7) Moveout velocities for reflection arrivals over azimuthally anisotropic media are abnormal unless the survey line is parallel to the fractures, or, more generally, parallel to a vertical invariant plane of the azimuthal anisotropy.

(8) Comparison of reflection amplitudes of corresponding events on the principal time series provides a measure, highly resolved in time, of local anisotropy differences; i.e., it allows one to see and characterize the fractures.

REFERENCES

Aki, K., and Richards, P. G., 1980, Quantitative seismology: Theory and methods: W. H. Freeman and Co.

Alford, R. M., 1986a, Multisource multireceiver method and system for geophysical exploration: European patent appl., no. 0 169 075.

——— 1986b, Shear data in the presence of azimuthal anisotropy: 56th Ann. Internat. Mtg., Soc. Explor. Geophys., Expanded Abstracts, 476–479.

Alford, R. M., Lynn, H. B., and Thomsen, L., 1986, Seismic survey technique for detection of azimuthal variations in the earth's subsurface: European patent appl. no. 0 169 076.

Backus, G. E., 1965, Possible forms of seismic anisotropy of the uppermost mantle under oceans: J. Geophys. Res., **70**, 3429.

Crampin, S., 1981, Review of wave motion in anisotropic and cracked elastic-media: Wave Motion, **3**, 343–391.

——— 1984a, An introduction to wave propagation in anisotropic media: Geophys. J. Roy. Astr. Soc., **76**, 17–28.

——— 1984b, Anisotropy in exploration seismics: First Break, **2**, no. 3, 19–21.

——— 1985a, Evaluation of anisotropy by shear-wave splitting: Geophysics, **50**, 142–152.

——— 1985b, Evidence for aligned cracks in the earth's crust: First Break, **3**, no. 3, 12–15.

——— 1986, Anisotropy and transverse isotropy: Geophys. Prosp., **34**, 94–99.

Crampin, S., Bush, I., Naville, C., and Taylor, D., 1986, Estimating the internal structure of reservoirs with shear-wave VSP's: Leading Edge, **5**, no. 11, 35.

Crampin, S., and Atkinson, B. K., 1985, Microcracks in the earth's crust: First Break, **3**, no. 3, 16–20.

Daley, P. F., and Hron, F., 1979, Reflection and transmission coefficients for seismic waves in ellipsoidally anisotropic media: Geophysics, **44**, 27–38.

Gajewski, D., and Psencik, I., 1988, Computation of high-frequency seismic wave fields in 3-D laterally inhomogeneous anisotropic media: To appear in Geophys. J. Roy. Astr. Soc.

Keith, C. M., and Crampin, S., 1977, Seismic body waves in anisotropic media: reflection and refraction at a plate interface: Geophys. J. Roy. Astr. Soc., **49**, 181–208.

Lynn, H. B., and Thomsen, L., 1986, Shear-wave exploration along the principal axes: 56th Ann. Internat. Mtg., Soc. Explor. Geophys., Expanded Abstracts, 473–476.

Martin, M. A., Davis, T. L., and O'Rourke, T. J., 1986, An integrated three-component approach to fracture detection: 56th Ann. Internat. Mtg., Soc. Explor. Geophys., Expanded Abstracts, 235–236.

Nye, J. F., 1957, Physical properties of crystals: Oxford Press.

Rai, C. S., and Hanson, K. E., 1986, Shear-wave birefringence: A laboratory study: 56th Ann. Internat. Mtg., Soc. Explor. Geophys., Expanded Abstracts, 471–473.

Thomsen, L., 1986a, Weak elastic anisotropy: Geophysics, **51**, 1954–1966.

——— 1986b, Reflection seismology in azimuthally anisotropic media: 56th Ann. Internat. Mtg., Soc. Explor. Geophys., Expanded Abstracts, 468–470.

Willis, H., Rethford, G., and Bielanski, E., 1986, Azimuthal anisotropy: Occurrence and effect on shear wave data quality: 56th Ann. Internat. Mtg., Soc. Explor. Geophys., Expanded Abstracts, 479–481.